JACS
JOURNAL OF THE AMERICAN CHEMICAL SOCIETY

Article

pubs.acs.org/JACS

A Thienoisoindigo-Naphthalene Polymer with Ultrahigh Mobility of 14.4 cm^2/V·s That Substantially Exceeds Benchmark Values for Amorphous Silicon Semiconductors

Gyoungsik Kim,[†,∥] Seok-Ju Kang,[‡,∥] Gitish K. Dutta,[†] Young-Kyu Han,[‡] Tae Joo Shin,[§] Yong-Young Noh,*[,‡] and Changduk Yang*[,†]

[†]School of Energy and Chemical Engineering, KIER-UNIST Advanced Center for Energy, Low Dimensional Carbon Materials Center, Ulsan National Institute of Science and Technology (UNIST), Ulsan 689-798, South Korea

[‡]Department of Energy and Materials Engineering, Dongguk University, 26 Pil-dong, 3 ga, Jung-gu, Seoul 100-715, South Korea

[§]Pohang Accelerator Laboratory, Pohang University of Science and Technology, Pohang, Kyungbuk 790-784, South Korea

Supporting Information

ABSTRACT: By considering the qualitative benefits associated with solution rheology and mechanical properties of polymer semiconductors, it is expected that polymer-based electronic devices will soon enter our daily lives as indispensable elements in a myriad of flexible and ultra low-cost flat panel displays. Despite more than a decade of research focused on designing and synthesizing state-of-the-art polymer semiconductors for improving charge transport characteristics, the current mobility values are still not sufficient for many practical applications. The confident mobility in excess of ∼10 cm^2/V·s is the most important requirement for enabling the realization of the aforementioned near-future products. We report on an easily attainable donor−acceptor (D−A) polymer semiconductor: poly(thienoisoindigo-*alt*-naphthalene) (PTIIG-Np). An unprecedented mobility of 14.4 cm^2/V·s, by using PTIIG-Np with a high-*k* gate dielectric poly(vinylidenefluoride-trifluoroethylene) (P(VDF-TrFE)), is achieved from a simple coating processing, which is of a magnitude that is very difficult to obtain with conventional TFTs by means of molecular engineering. This work, therefore, represents a major step toward truly viable plastic electronics.

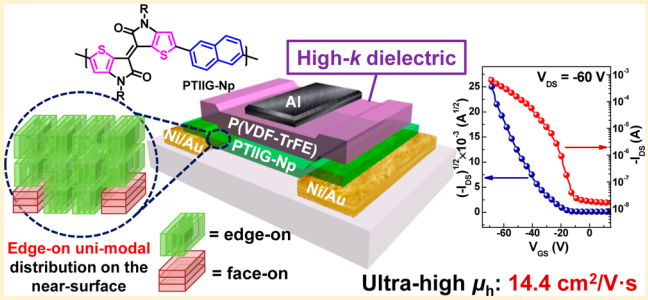

INTRODUCTION

High hopes exist for next-generation mobile displays, circuitry, and even radio frequency identification as well as e-paper,[1−4] each of which will doubtless have flexible, lightweight, large-area, and ultra-low-cost requirements.[3−13] By taking full advantage of their versatile chemical synthesis, superior processability from solutions at low temperatures, as well as mechanical flexibility/ruggedness that semiconducting polymers inherently possess, solution-printable polymer-based thin-film transistors (TFTs), both as discrete transistors and in integrated circuits,[14,15] are now regarded as an ideal candidate for meeting all the aforementioned prerequisites. Unquestionably, benefiting from the maturation of the donor−acceptor (D−A) polymer approaches, most recently, great progress in the field of polymer TFTs has yielded state-of-the-art materials with high charge-carrier mobilities, reliably exceeding 3 cm^2/V·s[16−19] and beyond for amorphous silicon semiconductors (a-Si:H, 0.5−1.0 cm^2/V·s).[20] Such a vigorous boost in TFTs performance is most frequently associated with the D−A frameworks in which either diketopyrrolopyrrole (DPP) or isoindigo (IIG), as a polar bicyclic lactam electron-deficient unit, was incorporated with electron-rich heteroacenes, such as thiophene and selenophene derivatives.[16−19,21−23]

Although exploring DPP- or IIG-based D−A polymers as well as shedding light on their high charge-carrier mobilities are still of great interest in the polymer academic community, the research in the area of these materials is almost reaching a plateau, threatened by development of strong alternative high-performance pigments. In a timely manner given the need for newer competitive materials, in 2012, McCulloch and co-workers disclosed a thiophene-implanted IIG unit, thienoisoindigo (TIIG), by modulating from the outer arylene groups of IIG to five-membered heterocyclic aromatic rings.[24] Consequently, the unique structural features of TIIG are capable of (i) improving coplanarity to the molecular plane via S···O interactions and (ii) enhancing the charge delocalization via a quinoidal structure of the backbone,[24−26] which can lead to better molecular ordering, π-conjugation, and charge transport efficiency.[5,27,28]

Shortly thereafter, it was widely expected that superior TFTs performance would be possible with a suitable molecular setup of TIIG-containing D−A systems, thus creating various TIIG-based polymer semiconductors with heteroacene building

Received: May 6, 2014
Published: June 10, 2014

dx.doi.org/10.1021/ja504537v | J. Am. Chem. Soc. 2014, 136, 9477−9483

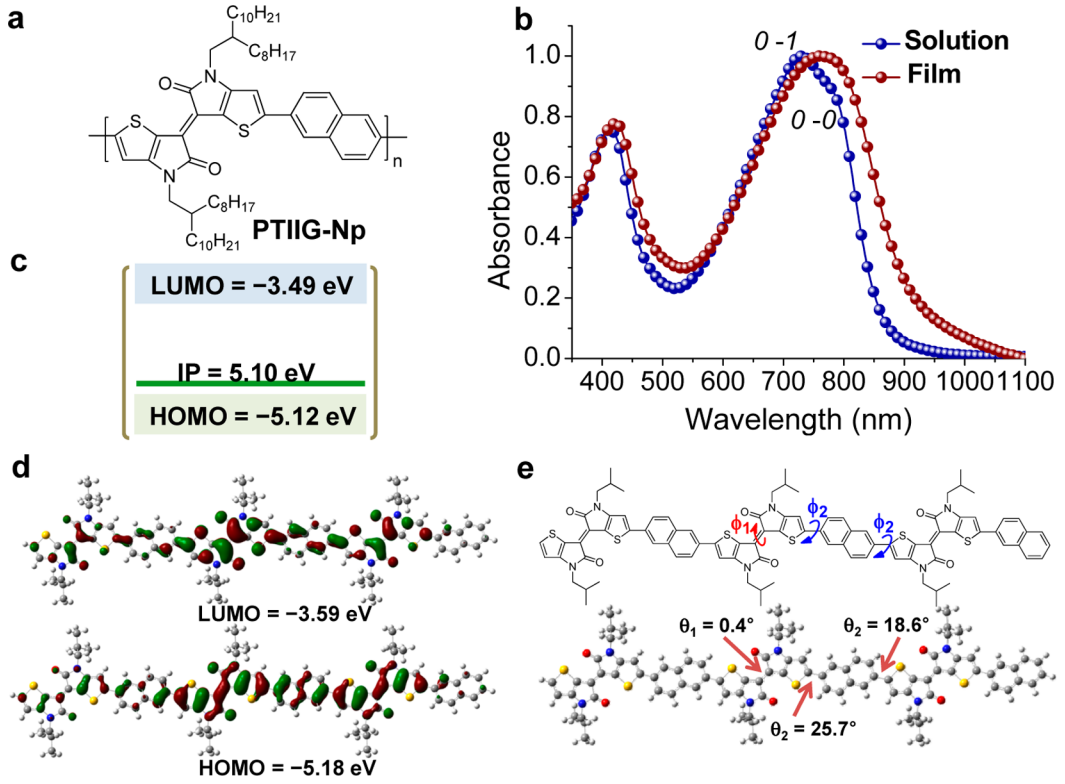

Figure 1. Chemical structure, ultraviolet absorption spectra, energy-level diagrams, and energy-minimized structure at the B3LYP/6-31G** level. (a) Structure of PTIIG-Np. (b) Normalized ultraviolet−visible absorption spectra of PTIIG-Np in $CHCl_3$ solution and as a thin film on quartz substrate. (c) HOMO and LUMO levels determined by the thin films using cyclic voltammetry (CV) calibrated by the Fc/Fc^+ redox couple as an external standard. IP was also measured by ultraviolet photoelectron spectroscopy (UPS) technique. (d) DFT-optimized geometries and charge-density isosurfaces for the trimeric system with a visualization of the HOMO and LUMO molecular orbitals (green and red represent the isosurfaces (iso value = 0.02) of the opposite phase of the wave functions). (e) Calculated dihedral angles of the trimer structure.

blocks as a novel polymer design. Disappointingly, it turned out that the observed mobilities were no greater than ~0.3 $cm^2/V{\cdot}s$,[24−26,29] which was 1−3 orders of magnitude lower than those obtained for current DPP- or IIG-containing semiconductors. This is probably due to the suppression of the full potential merits of TIIG unit within such structures, rather than its intrinsic property limitations; nevertheless, it is undeniably a setback for in this field. Very recently, we found that the geometric skeletons of the donors in D−A polymers with an identical acceptor could reflect the interchain $\pi-\pi$ stacking as well as carrier mobility dynamics, rather than inserting electron-rich heteroacene donors into the backbone to further strengthen intramolecular charger transfer.[30]

Herein, we depart from the common choice of the heteroacene-based donors and focus on employing acene-based centrosymmetric donor unit for TIIG-based platform. Using commercially available naphthalene (Np) as the simplest fused centrosymmetric acene, we present an easily accessible TIIG-containing D−A polymer, poly(thienoisoindigo-*alt*-naphthalene) (abbreviated as PTIIG-Np, see Figure 1a for its molecular structure), and comprehensively describe its thin-film properties and transistor characteristics. PTIIG-Np shows excellent *p*-type dominant TFTs performance, with hole mobility of 5.8 $cm^2/V{\cdot}s$ employing common poly(methyl methacrylate) (PMMA) dielectric in a top gate structure. Furthermore, an unprecedented mobility of up to 14.4 $cm^2/V{\cdot}s$ is achieved from the PTIIG-Np TFTs adopting a high-*k* gate polymer dielectric poly(vinylidenefluoride-trifluoroethylene) (P(VDF-TrFE)), which is the highest mobility value among lactam-based polymers reported in the literature so far.

RESULTS AND DISCUSSION

Synthetic Strategies, Synthesis, and Characterization. Our target polymer, PTIIG-Np (Figure 1a), was synthesized via Pd-catalyzed Suzuki polymerization between (*E*)-2,2′-dibromo-4,4′-bis(2-octyldodecyl)-[6,6′-bithieno[3,2-*b*]pyrrolylidene]-5,5′(4*H*,4′*H*)-dione and 2,6-bis(4,4,5,5-tetramethyl-1,3,2-dioxaborolan-2-yl)naphthalene, followed by Soxhlet extraction to remove impurities and undesired molecular weight fractions (see Scheme 1 for polymerization and syntheses of all the intermediates and their characterizations in Supporting Information). PTIIG-Np (M_n = 21.0 kDa using PS/THF standard) has excellent solubility in common organic solvents (THF, chloroform, toluene, etc.) and forms uniform thin films by spin-coating. As depicted in Figure 1b, PTIIG-Np shows dual-band absorptions in the region of 330−1100 nm, covering the whole visible to near-infrared range. Compared to those in solution, the absorption peaks of the thin films are not only red-shifted, but the intensity of 0−0 vibrational transition relative to 0−1 is also increased, thus becoming a broader band at the low-energy region. This indicates that the molecules in solid state undergo molecular organization to form more ordered structures, most likely as a result of the strong D−A interactions.

Cyclic voltammetry was used to estimate the frontier molecular orbital energy levels (Figure S1, Supporting Information). The highest occupied molecular orbital

dx.doi.org/10.1021/ja504537v | *J. Am. Chem. Soc.* 2014, 136, 9477−9483

Scheme 1. Synthetic Routes of PTIIG-Np[a]

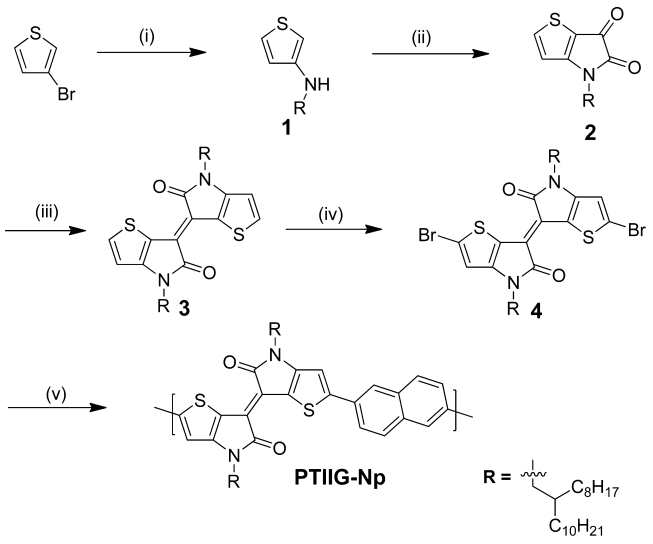

[a]Reagents and conditions: (i) 2-Octyldodecane-1-amine, Cu, CuI, K_3PO_4, dimethyl aminoethanol, reflux, 48 h, 41%; (ii) Oxalyl chloride, triethylamine, DCM, rt, overnight, 40%; (iii) Lawesson's reagent, toluene, 60 °C, 2 h, 35%; (iv) NBS, THF, rt, overnight, 70%; (v) Suzuki polymerization, 2,6-bis(4,4,5,5-tetramethyl-1,3,2-dioxaborolan-2-yl)naphthalene, toluene, H_2O, K_3PO_4, P(*o*-tolyl)$_3$, $Pd_2(dba)_3$, 90 °C, 72 h, 59%.

(HOMO) and lowest unoccupied molecular orbital (LUMO) levels are estimated to be −5.12 and −3.49 eV, respectively (Figure 1c). The ionization potential (IP, |HOMO|) of PTIIG-Np, measured by ultraviolet photoelectron spectroscopy (UPS) in air, is also found to be ca. −5.10 eV (see Figure S2, Supporting Information), which is notably greater than that of P3HT (∼−4.7 eV), often referred to as the "fruit fly" of organic semiconductors.[7,31] The low-lying HOMO energy level is expected to be beneficial for increasing ambient stability of the polymer against oxidation as well as reducing the hole injection barrier between a gold source electrode and *p*-type semiconductor, which consequently would improve the device performance.

Upon B3LYP/6-31G** calculation on the trimer length oligomer with isobutyl groups, it is apparent that the HOMO is delocalized along the polymer chain, whereas the LUMO is somewhat concentrated on the TIIG core (Figure 1d). Thus, the nature of PTIIG-Np is considering *p*-channel dominant ambipolar TFT characteristics achievable (vide infra). The HOMO/LUMO energies obtained from the calculations of IP and optical bandgap are −5.10/−3.74 eV and in very close agreement with the experimental data. In addition, this reveals that the intra twist (θ_1) within centrosymmetric ketopyrrole cores is ≤0.4°, while the inter torsion (θ_2) of 18.6−25.7° exists between TIIG and neighboring Np subunits (Figure 1e).

Fabrication of Solution-Processed TFTs and I−V Characterizations. We built high-performance TFT devices using PTIIG-Np polymer film (from 1,2,4-trichlorobenzene solution, ∼5 mg mL^{-1}). The devices were fabricated in a top-gate and bottom-contact (TG-BC) configuration, with prepatterned Ni (t ∼ 3 nm) /Au (t ∼ 12 nm) source-drain electrodes and PMMA acting as the gate dielectric, which was then spin-cast onto the polymer semiconductor layer. To explore the thermally induced PTIIG-Np ordering effect, the semiconductor layers were annealed at various temperatures (80, 150, 200, 250, and 310 °C) before spin-coating the dielectric layer. Al gate electrode was then deposited by thermal evaporation to complete the TFT structure.

In prepatterned electrodes, the channel width (W) and length (L) are 1 mm and 20 μm for the devices with PMMA (Figure 2a). Device fabrication and characterization were performed in a nitrogen gas filled glovebox (oxygen and moisture <20 ppm). The experimental details regarding TFT fabrication and surface modification are described in the Supporting Information. Figure 2b exhibits the transfer curves tested from the PTIIG-Np TFTs with PMMA dielectric layer, showing *p*-type dominant ambipolar characteristics, and their electrical properties are summarized in Table 1. As the annealing temperature (ranging from 80 to 310 °C) was increased, gradually enhanced charge-carrier mobilities were observed at both hole and electron, resulting in the hole and electron mobilities (μ_h and μ_e) of up to 5.8 and 0.092 cm^2/V·s, respectively, from the 310 °C annealed film. Over 20 devices from four different substrates were measured, and the average μ_h and μ_e extracted from the saturation regime were 4.9 and 0.057 cm^2/V·s, respectively, for these devices. To our knowledge, this is the highest value among TIIG-based polymers reported to date. Additionally, we observed a relatively reduced contact resistances (R_c·W) for the hole injection upon the PTIIG-Np films annealed at 150−310 °C (<6 × 10^{-5} Ω·cm) compared to the case of 80 °C (1−5 × 10^{-6} Ω·cm) (Table 1 and Figure S4b, Supporting Information), which implies better intimate physical contact and molecular chain orientation between the semiconductors and the S−D electrodes by the thermal annealing process.

An intriguing question that arises here is whether the TIIG building block within the polymer framework is critical for the excellent TFT performance. To address this open question, we fabricated the TG-BC TFTs using the corresponding IIG-based polymer (PIIG-Np) as a semiconductor (see synthesis and structure in Scheme S1, Supporting Information). The devices based on this polymer exhibited about 100 times lower hole mobilities (μ_h = ∼10^{-2} cm^2/V·s) than those of PTIIG-Np, which is associated with the large differences between two semiconductors in the respect of energy levels and conjugated backbone planarity (Figure S5 and Table S2, Supporting Information). Therefore, the origin of the overall improved PTIIG-Np transistor performance could be ascribed to the structural and electronic features originating from the suitable molecular setup.

It is true that the nature of the microscopic motion of charge carriers has been correlated to the chemical purity and structural quality of the organic semiconductors. The fact that the dielectric properties of the gate insulator also have a strong influence on the charge mobility has been discovered recently.[13,32,33] Although the extraordinary mobilities were achieved as described above, here we still decided to construct the TFT devices (W = 1 mm, L = 50 μm) of PTIIG-Np based on the optimized annealing temperature (310 °C) by replacing PMMA layer with P(VDF-TrFE). P(VDF-TrFE), a well-known a high-dielectric-constant ("high-*k*", k = 10−12) ferroelectric polymer, resulting in lower operating voltages of TFTs,[34,35] which is especially desirable for portable and wearable electronics.[3,36,37] Moreover, our group recently demonstrated a significant enhancement of hole transport and injection for *n*-channel dominant naphthalene-bis(dicarboximide)-dithiophene polymer (P(NDI2OD-T2)) using P(VDF-TrFE) in which well-balanced ambipolarity being mobile for both holes and

dx.doi.org/10.1021/ja504537v | J. Am. Chem. Soc. 2014, 136, 9477−9483

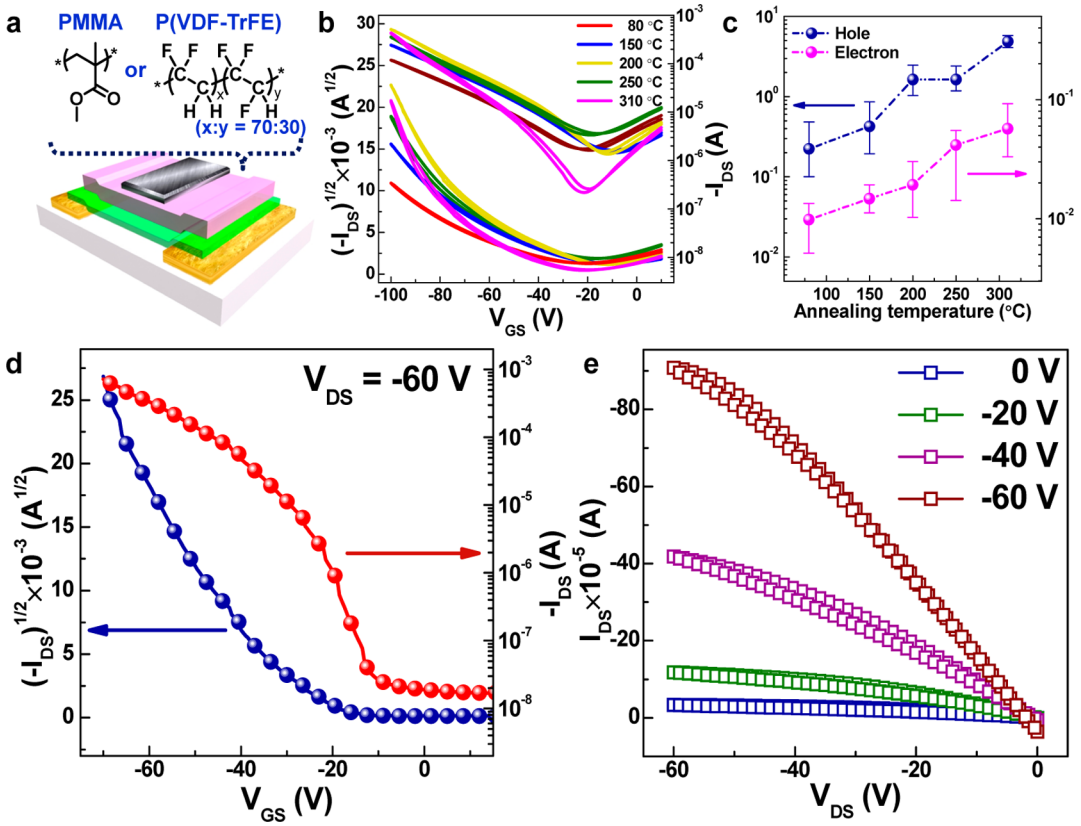

Figure 2. Device geometry of solution-processed PTIIG-Np TFTs and their electrical characteristics. (a) Schematic cross-section of the top-gate and bottom-contact (TG-BC) geometry and the chemical structures of PMMA and P(VDF-TrFE) as the gate dielectric layer. (b,c) Transfer curves of PTIIG-Np devices with PMMA dielectric at −100 V of V_{DS} (channel width (W): 1 mm, length (L): 20 μm), of which semiconductor films were annealed at different temperatures (b) and hole and electron charge-carrier mobility (cm^2/V·s) distributions based on various annealing temperatures (c). (d,e) Transfer (d) and output (e) characteristics for PTIIG-Np TFTs after thermal annealing at 310 °C with P(VDF-TrFE) gate insulator (channel width (W): 1 mm, length (L): 50 μm), where the devices were additionally cured at 160 °C after spin-coating of the gate dielectric layer on the top of semiconductor surface, in order to suppress the crystalline β-phase induced by the large ferroelectric properties.

Table 1. Summary of TFT Performance Characteristics for PTIIG-Np Semiconductor with Different Gate Dielectrics

condition[a]		*p*-channel				*n*-channel		
insulator (thickness)	T [°C]	$\mu_{h,max}$ [cm^2/V·s]	$\mu_{h,avg}$ [cm^2/V·s]	V_{th} [V]	$R_c{\cdot}W$ [Ω·cm]	$\mu_{e,max}$ [cm^2/V·s]	$\mu_{e,avg}$ [cm^2/V·s]	V_{th} [V]
PMMA (~500 nm)[b]	80	0.48	0.22	−48 to −59	1.18−4.67 × 10^6	0.013	0.0098	56−65
	150	0.86	0.43	−51 to −58	2.15−2.20 × 10^5	0.019	0.015	59−63
	200	2.5	1.6	−59 to −67	1.34−1.84 × 10^5	0.030	0.019	55−71
	250	2.4	1.6	−64 to −69	1.24−2.57 × 10^5	0.055	0.042	54−69
	310	5.8	4.9	−74 to −79	0.81−5.83 × 10^5	0.092	0.057	62−75
P(VDF-TrFE) (~600 nm)[b]	310	14.4	12.0	−45 to −48	3.20−4.10 × 10^3		N.A.	

[a]The TFT performance of more than 20 devices was tested in nitrogen atmosphere. [b]The capacitance values per unit area of PMMA and P(VDF-TrFE) were calculated as 6.2 and 15.5 nF/cm^2, respectively.

electrons (~0.1 cm^2/V·s) was realized.[38] The TG-BC PTIIG-Np devices were fabricated similarly to the former case, except that high-k P(VDF-TrFE) was used as the gate dielectric layer after spin-coating the semiconductor solution and then applying the optimized annealing temperature of 310 °C for semiconductor ordering (see Figure 2d and Figure 2e). Consequently, after spin-coating of P(VDF-TrFE) solution, the films were baked at 80 °C to remove the residual solvent, and the completed devices were reheated at 160 °C above the melting temperature (T_m: ~148 °C) in order to get rid of its crystalline β-phase formation,[39] of which state would induce the large ferroelectric properties in P(VDF-TrFE). The β-phase peak of a P(VDF-TrFE) film at ca. 20° in the diffraction angle was fully diminished by the melt-annealing process (at 160 °C) (see Figure S8, Supporting Information). As contrasted to the PMMA dielectric case with PTIIG-Np TFTs, the devices based on P(VDF-TrFE) rendered unipolar *p*-type operations, with unprecedented high mobility of up to 14.4 cm^2/V·s (12 cm^2/V·s on average), which could be promising for real-life TFTs. In our previous report, the origin of the remarkable boost in the hole carrier mobility was explained by the molecular orbital energy modulation through dipoles of P(VDF-TrFE) and organic semiconductor, which pull-up HOMO and LUMO levels.[38] Thus, the large dipole polarization at the interface of the fluorinated polymer can promote the accumulation of positive charge carriers at the semiconductor-dielectric interlayer by the band bending.

dx.doi.org/10.1021/ja504537v | J. Am. Chem. Soc. 2014, 136, 9477−9483

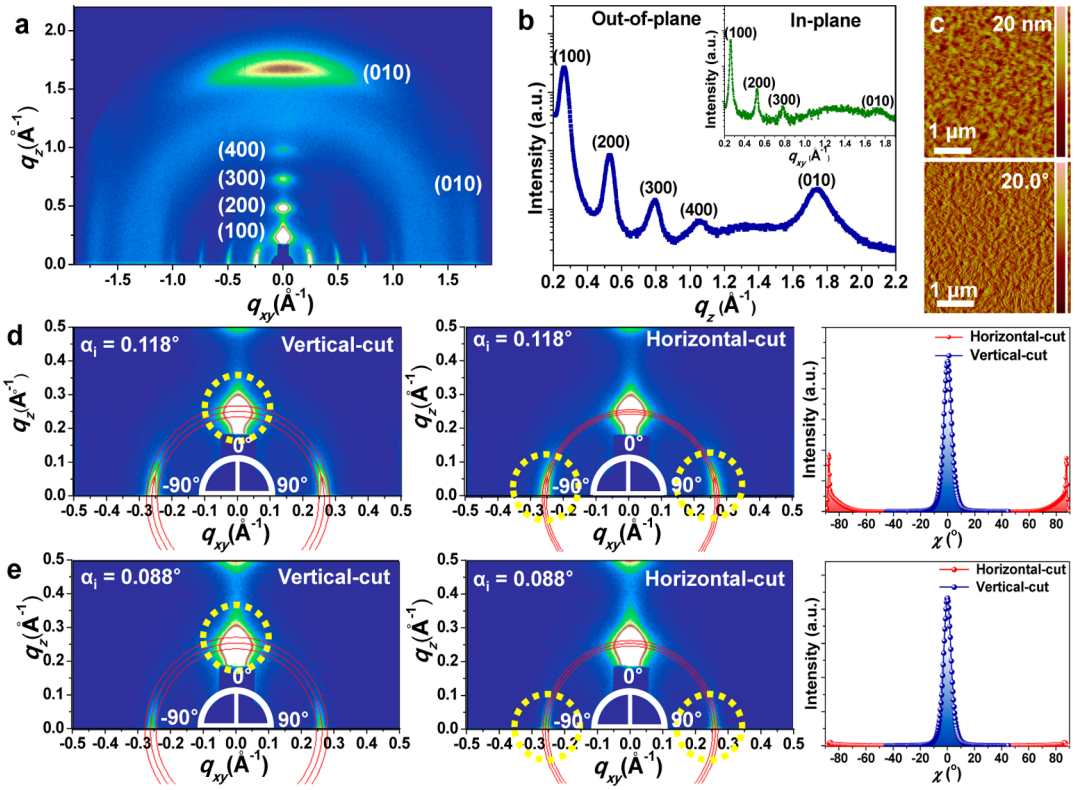

Figure 3. Microstructure analysis of PTIIG-Np. GIXD profiles and AFM images of solution-processed PTIIG-Np films annealed at 310 °C. (a,b) 2D-GIXD images (a) and 1D out-of-plane GIXD profile (b) of thin films (inset is the corresponding in-plane GIXD profile). (c) AFM height (top) and phase (bottom) images. (d,e) The local GIXD data ranged from −0.5 to 0.5 Å^{-1} in q_{xy} and from 0 to 0.5 Å^{-1} in q_z and the corresponding intensity-corrected pole figures of the (100) reflection. Data in (d) are the diffractions in which the incidence angle of X-ray was set to be 0.118°, just above the critical angle of the film but below the critical angle of the substrate, to penetrate whole film thickness. Data in (e) are the diffractions in which the incidence angle of X-ray was set to be 0.088°, below the critical angle of the film, to explore the majority populations on the near-surface region of the film. The columns on the left and the middle qualitatively represent the circular averaged areas along $q_{xy} \approx 0$ Å^{-1} (fraction of edge-on crystallites) and $q_z \approx 0$ Å^{-1} (fraction of face-on crystallites), respectively. The columns on the right show the complete pole figures, compiled by the integral intensities from each area (where χ is defined as the angle between the crystallite orientation and the surface normal).

Thin Film Microstructure Analyses. To gain a picture of the correlation between molecular packing/crystallinity and the unprecedented TFTs performance, we investigated the microstructure (crystalline nature and molecular orientation) of PTIIG-Np, based on grazing incidence X-ray diffraction (GIXD) and atomic force microscopy (AFM) measurements. Figures 3a and 3b show the 2D-GIXD image and extracted in- and out-of-plane GIXD profiles) of the PTIIG-Np films annealed at 310 °C prepared by spin-casting onto SiO_2/Si substrate. The GIXD patterns at different temperatures (80, 150, 200, and 250 °C) are provided in Figure S9 (Supporting Information). The detailed crystallographic parameters extracted from those GIXD patterns are also listed in Table S4 (Supporting Information).

The GIXD reveals that every PTIIG-Np film has well-ordered layer-by-layer lamellar packing microstructure, adopting bimodal distribution of edge-on and face-on crystallites, where the molecular packing out-of-plane appears nominally along the q_z axis and the in-plane ordering along q_{xy}. Along the out-of-plane direction, almost all polymer films exhibit the diffraction peaks up to the fourth order of the lamellar stacking repeat (i.e., (100), (200), (300), and (400); d_{100} = 23.8−25.8 Å) with additional multiple-diffracted intensities also observed in in-plane direction. In addition, the short π−π stacking spacings of ∼3.6 Å (q = ∼1.7 Å^{-1}) in both q_z and q_{xy} profiles are obtained from all case films (assigned as (010) peak here), being convincing evidence of 3-D conduction channel-induced structures. As the thermal annealing was increased up to 250 °C, no significant changes in the diffraction patterns were observed, while in both the q_z and q_{xy}, there is not only a slight shift in the (100) peak position to higher values (∼sub-Å range), but also its estimated coherence length (L_c) based on Scherrer's equation[40] is gradually increased. Especially, after annealing the films to 310 °C, the diffraction peaks become more-intense and sharper, leading to remarkably large (100) L_c values of 140 Å (q_z axis) and 383 Å (q_{xy} axis) (compared to those annealed at different temperatures), which indicates further improved microstructural ordering and enhanced crystalline structure.[41,42] Therefore, these GIXD data support the observed highest performance for PTIIG-Np film annealed at 310 °C.

Moreover, to quantify the difference between the edge-on and face-on populations in the film annealed at 310 °C, we constructed a pole figure for the (100) reflection, and extracted the integrated intensity as a function of χ along the arcs, where χ (−90° to 90°) is defined as the semicircular angle between the crystallite orientation and the surface normal.[43] The diffraction data and intensity-corrected pole figure are plotted in Figure 3d. The peaks in intensity near χ = 0° (vertical-cut) and near χ = ± 90° (horizontal-cut) are associated with the edge-on and face-on crystallites, respectively. The area ratio of the two peaks (χ = 0°−45° and χ = 45°−90°) is ≈7:3 (71.2%

dx.doi.org/10.1021/ja504537v | J. Am. Chem. Soc. 2014, 136, 9477−9483

vs 28.8%), implying a majority edge-on crystallite population in the entire film thickness since the incidence angle (α_i = 0.118°) used is just above the critical angle, ensuring that we sampled the full film depth. On the other hand, when the incidence angle (α_i = 0.088°) is set lower than the sample's critical angle, for accessing majority populations on the near-surface region of the film, the bimodal distribution is changed to almost unimodal distribution of the edge-on structure (97.6%) with the trace amount of the face-on structure (see Figure 3e). These findings signify that the region near the top surface of the polymer film has a stronger preference for the edge-on orientation compared to that of close to the substrate regions. Therefore, TG-BC TFT architecture used here is thought to be an ideal fit for achieving high mobility of PTIIG-Np, because, in general, the edge-on structure is considered favorable for charge transport.[44,45] The very lower mobilities (μ_h = ~10^{-2} $cm^2/V{\cdot}s$) in the PTIIG-Np-based bottom-gate and top-contact (BG-TC) devices clearly confirmed the dependence of the device geometry (Figure S10 and Table S5, Supporting Information).

As shown in Figure 3c, the AFM images illustrate that the film annealed at 310 °C consists of uniform polymer fibers that establish highly aligned nanofibrillar networks (see Figure S11, Supporting Information, for the AFM images at different temperatures). The densely ordered structures are likely due to closer $\pi-\pi$ stacking of polymer chains, similarly to other high-performance TFTs materials.[16,17,46−48] We believed that the tightened conformation could also play a critical role in the charge transport efficacy via hopping mechanism.

CONCLUSIONS

In order to meet the need for real-life TFTs based on polymer semiconductors as the linchpin of next-generation electronic devices, we present an easily synthesized D−A semiconducting polymer based on alternating the recently formulated thienoisoindigo (TIIG) and simple naphthalene (Np) units, PTIIG-Np, and investigate to determine application in TFTs. PTIIG-Np offers favorable property of charge-carrier mobility (up to 5.8 $cm^2/V{\cdot}s$) thanks to its inherently large coplanarity, favorable energetic levels for hole injection, as well as ideal film morphology that improves semicrystalline lamellar ordering and $\pi-\pi$ stacking to achieve a high charge-hopping rate between the polymer chains. More surprisingly, an ultrahigh mobility of 14.4 $cm^2/V{\cdot}s$ is demonstrated for the TFT devices using PTIIG-Np with a high-k P(VDF-TrFE). This finding is sharply distinguished from most p-type organic semiconductors, which exhibit lower mobilities for higher gate dielectric constant. This charge-transport efficacy far beyond the current levels essentially comes courtesy of a winning combination of the rational design of the polymer backbone, the optimal selection of the device configuration, and the benign dielectric-molecule dynamics. Not only does this value by far exceed those of both amorphous silicon semiconductors and solution-processed small molecular counterparts, but it is also competitive with the performance of TFTs based on organic single crystals and transparent metal oxides. Therefore, this result shows the power of important progress for solution-processed polymer TFTs and spurs technological translation of practical plastic electronics from laboratory to marketplace.

ASSOCIATED CONTENT

Supporting Information

Detailed experimental procedures and characterization for polymer as well as the device fabrication procedures, measurements, and additional figures (cyclic voltammetry plots, UPS spectroscopy, temperature- and structure-dependence TFTs characteristics, additional AFM and GIXD images). This material is available free of charge via the Internet at http://pubs.acs.org.

AUTHOR INFORMATION

Corresponding Authors

yynoh@dongguk.edu
yang@unist.ac.kr

Author Contributions

‖G. Kim and S.-J. Kang contributed equally.

Notes

The authors declare no competing financial interest.

ACKNOWLEDGMENTS

This research was supported by the Basic Science Research Program through the National Research Foundation of Korea (NRF) funded by the Korean Ministry of Science, ICT, and Future Planning (Grant No.: 2013R1A1A1A05004475, 2010-0019408, BK21 Plus (10Z20130011057)). This research was also supported by the International Cooperation of the Korea Institute of Energy Technology Evaluation and Planning (KETEP) grant funded by the Korean Ministry of Knowledge Economy (2012T100100740), the Center for Advanced Soft-Electronics funded by the Ministry of Science, ICT, and Future Planning as Global Frontier Project (2013M3A6A5073183), and by the Dongguk University Research Fund of 2013. Experiments at PLS-II 9A U-SAXS beamline were supported in part by MEST and POSTECH.

REFERENCES

(1) Beaujuge, P. M.; Fréchet, J. M. *J. Am. Chem. Soc.* **2011**, *133*, 20009.
(2) Gelinck, G.; Heremans, P.; Nomoto, K.; Anthopoulos, T. D. *Adv. Mater.* **2010**, *22*, 3778.
(3) Arias, A. C.; MacKenzie, J. D.; McCulloch, I.; Rivnay, J.; Salleo, A. *Chem. Rev.* **2010**, *110*, 3.
(4) Yan, H.; Chen, Z.; Zheng, Y.; Newman, C.; Quinn, J. R.; Dötz, F.; Kastler, M.; Facchetti, A. *Nature* **2009**, *457*, 679.
(5) Sirringhaus, H.; Brown, P.; Friend, R.; Nielsen, M. M.; Bechgaard, K.; Langeveld-Voss, B.; Spiering, A.; Janssen, R. A.; Meijer, E.; Herwig, P. *Nature* **1999**, *401*, 685.
(6) Tsao, H. N.; Cho, D. M.; Park, I.; Hansen, M. R.; Mavrinskiy, A.; Yoon, D. Y.; Graf, R.; Pisula, W.; Spiess, H. W.; Müllen, K. *J. Am. Chem. Soc.* **2011**, *133*, 2605.
(7) McCulloch, I.; Heeney, M.; Bailey, C.; Genevicius, K.; MacDonald, I.; Shkunov, M.; Sparrowe, D.; Tierney, S.; Wagner, R.; Zhang, W. *Nat. Mater.* **2006**, *5*, 328.
(8) Pan, H.; Li, Y.; Wu, Y.; Liu, P.; Ong, B. S.; Zhu, S.; Xu, G. *J. Am. Chem. Soc.* **2007**, *129*, 4112.
(9) Dhoot, A. S.; Yuen, J. D.; Heeney, M.; McCulloch, I.; Moses, D.; Heeger, A. J. *Proc. Natl. Acad. Sci. U. S. A.* **2006**, *103*, 11834.
(10) Briseno, A. L.; Mannsfeld, S. C.; Ling, M. M.; Liu, S.; Tseng, R. J.; Reese, C.; Roberts, M. E.; Yang, Y.; Wudl, F.; Bao, Z. *Nature* **2006**, *444*, 913.
(11) Muccini, M. *Nat. Mater.* **2006**, *5*, 605.
(12) Dimitrakopoulos, C.; Purushothaman, S.; Kymissis, J.; Callegari, A.; Shaw, J. *Science* **1999**, *283*, 822.
(13) Hulea, I.; Fratini, S.; Xie, H.; Mulder, C.; Iossad, N.; Rastelli, G.; Ciuchi, S.; Morpurgo, A. *Nat. Mater.* **2006**, *5*, 982.
(14) Brown, A.; Pomp, A.; Hart, C.; De Leeuw, D. *Science* **1995**, *270*, 972.
(15) Crone, B.; Dodabalapur, A.; Lin, Y.-Y.; Filas, R.; Bao, Z.; LaDuca, A.; Sarpeshkar, R.; Katz, H.; Li, W. *Nature* **2000**, *403*, 521.

(16) Lee, J.; Han, A.-R.; Yu, H.; Shin, T. J.; Yang, C.; Oh, J. H. *J. Am. Chem. Soc.* **2013**, *135*, 9540.
(17) Lee, J.; Han, A.-R.; Kim, J.; Kim, Y.; Oh, J. H.; Yang, C. *J. Am. Chem. Soc.* **2012**, *134*, 20713.
(18) Li, J.; Zhao, Y.; Tan, H. S.; Guo, Y.; Di, C.-A.; Yu, G.; Liu, Y.; Lin, M.; Lim, S. H.; Zhou, Y. *Sci. Rep.* **2012**, *2*, 754.
(19) Chen, H.; Guo, Y.; Yu, G.; Zhao, Y.; Zhang, J.; Gao, D.; Liu, H.; Liu, Y. *Adv. Mater.* **2012**, *24*, 4618.
(20) Sirringhaus, H. *Adv. Mater.* **2005**, *17*, 2411.
(21) Lei, T.; Dou, J. H.; Pei, J. *Adv. Mater.* **2012**, *24*, 6457.
(22) Mei, J.; Kim, D. H.; Ayzner, A. L.; Toney, M. F.; Bao, Z. *J. Am. Chem. Soc.* **2011**, *133*, 20130.
(23) Lei, T.; Cao, Y.; Fan, Y.; Liu, C.-J.; Yuan, S.-C.; Pei, J. *J. Am. Chem. Soc.* **2011**, *133*, 6099.
(24) Ashraf, R. S.; Kronemeijer, A. J.; James, D. I.; Sirringhaus, H.; McCulloch, I. *Chem. Commun.* **2012**, *48*, 3939.
(25) Koizumi, Y.; Ide, M.; Saeki, A.; Vijayakumar, C.; Balan, B.; Kawamoto, M.; Seki, S. *Polym. Chem.* **2013**, *4*, 484.
(26) Van Pruissen, G. W.; Gholamrezaie, F.; Wienk, M. M.; Janssen, R. A. *J. Mater. Chem.* **2012**, *22*, 20387.
(27) Chabinyc, M. L.; Toney, M. F.; Kline, R. J.; McCulloch, I.; Heeney, M. *J. Am. Chem. Soc.* **2007**, *129*, 3226.
(28) DeLongchamp, D. M.; Kline, R. J.; Lin, E. K.; Fischer, D. A.; Richter, L. J.; Lucas, L. A.; Heeney, M.; McCulloch, I.; Northrup, J. E. *Adv. Mater.* **2007**, *19*, 833.
(29) Dutta, G. K.; Han, A.-R.; Lee, J.; Kim, Y.; Oh, J. H.; Yang, C. *Adv. Funct. Mater.* **2013**, *23*, 5317.
(30) Kim, Y.; Hong, J.; Oh, J. H.; Yang, C. *Chem. Mater.* **2013**, *25*, 3251.
(31) Hou, J.; Tan, Z. a.; Yan, Y.; He, Y.; Yang, C.; Li, Y. *J. Am. Chem. Soc.* **2006**, *128*, 4911.
(32) Xia, Y.; Cho, J. H.; Lee, J.; Ruden, P. P.; Frisbie, C. D. *Adv. Mater.* **2009**, *21*, 2174.
(33) Veres, J.; Ogier, S. D.; Leeming, S. W.; Cupertino, D. C.; Mohialdin Khaffaf, S. *Adv. Funct. Mater.* **2003**, *13*, 199.
(34) Naber, R. C.; Tanase, C.; Blom, P. W.; Gelinck, G. H.; Marsman, A. W.; Touwslager, F. J.; Setayesh, S.; De Leeuw, D. M. *Nat. Mater.* **2005**, *4*, 243.
(35) Li, J.; Sun, Z.; Yan, F. *Adv. Mater.* **2012**, *24*, 88.
(36) Sekitani, T.; Zschieschang, U.; Klauk, H.; Someya, T. *Nat. Mater.* **2010**, *9*, 1015.
(37) Gundlach, D. J. *Nat. Mater.* **2007**, *6*, 173.
(38) Baeg, K. J.; Khim, D.; Jung, S. W.; Kang, M.; You, I. K.; Kim, D. Y.; Facchetti, A.; Noh, Y. Y. *Adv. Mater.* **2012**, *24*, 5433.
(39) Mao, D.; Quevedo-Lopez, M.; Stiegler, H.; Gnade, B.; Alshareef, H. *Org. Electron.* **2010**, *11*, 925.
(40) Patterson, A. *Phys. Rev.* **1939**, *56*, 978.
(41) Rivnay, J.; Noriega, R.; Northrup, J. E.; Kline, R. J.; Toney, M. F.; Salleo, A. *Phys. Rev. B: Condens. Matter Mater. Phys.* **2011**, *83*, 121306.
(42) Zhang, X.; Bronstein, H.; Kronemeijer, A. J.; Smith, J.; Kim, Y.; Kline, R. J.; Richter, L. J.; Anthopoulos, T. D.; Sirringhaus, H.; Song, K.; Heeney, M.; Zhang, W.; McCulloch, I.; DeLongchamp, D. M. *Nat. Commun.* **2013**, *4*, 2238.
(43) Rivnay, J.; Steyrleuthner, R.; Jimison, L. H.; Casadei, A.; Chen, Z.; Toney, M. F.; Facchetti, A.; Neher, D.; Salleo, A. *Macromolecules* **2011**, *44*, 5246.
(44) Schuettfort, T.; Thomsen, L.; McNeill, C. R. *J. Am. Chem. Soc.* **2013**, *135*, 1092.
(45) Caironi, M.; Bird, M.; Fazzi, D.; Chen, Z.; Di Pietro, R.; Newman, C.; Facchetti, A.; Sirringhaus, H. *Adv. Funct. Mater.* **2011**, *21*, 3371.
(46) Usta, H.; Newman, C.; Chen, Z.; Facchetti, A. *Adv. Mater.* **2012**, *24*, 3678.
(47) Yuen, J. D.; Fan, J.; Seifter, J.; Lim, B.; Hufschmid, R.; Heeger, A. J.; Wudl, F. *J. Am. Chem. Soc.* **2011**, *133*, 20799.
(48) Bronstein, H.; Chen, Z.; Ashraf, R. S.; Zhang, W.; Du, J.; Durrant, J. R.; Shakya Tuladhar, P.; Song, K.; Watkins, S. E.; Geerts, Y. *J. Am. Chem. Soc.* **2011**, *133*, 3272.